

Treatment of Cancer by Radiotherapy and Nanoparticles Coupled With Methotrexate

Sahar E. Abo-Neima^{1*}, Abdelrahman S. Ismail², Hussein A. Motaweh¹

1. Physics Department, Faculty of Science, Damanhour University, Egypt.
2. Physics Department, Faculty of Applied Medical Science, Pharos University, Egypt.

ARTICLE INFO	ABSTRACT
<p>Article type: Original Paper</p>	<p>Introduction: Cancer patients receive radiation therapy (RT) as part of their treatment as monotherapy or as part of a combination treatment. Radiation therapy uses high-energy radiation such as photons and strong ions. Nanoparticles (NPs) are used for magnetic hyperthermia, which increases the efficacy of RT and generates heat to kill cancer cells by destroying their DNA.</p> <p>Material and Methods: Nanoparticles were prepared using the co-precipitation method and characterized using transmission electron microscopy (TEM), scanning electron microscopy (SEM), and X-ray diffractometer. Fifty-six male mice were housed under similar environmental conditions. The animals were injected into the right flank with 0.25 mL of 10^6 cells/mL Ehrlich tumor suspension. When tumors reached 5-10 mm in diameter, the mice were randomly divided into eight groups as follows: 1st group: used as the control group injected with 25 μL of phosphate buffer saline without treatment, 2nd group: injected with Fe_3O_4-NPs, 3rd group: injected with Fe_2O_3-NPs, 4th group: injected with methotrexate (MTX), 5th group: injected with MTX, Fe_3O_4, and Fe_2O_3-NPs, 6th group: as the 5th group with microwave hyperthermia, 7th group: as the 5th group then treated with high-energy photons, and 8th group: as the 5th group and exposed to electron beam therapy. Tumor volume and weight were measured after 15 days. Tumor apoptosis was studied using histopathology, and the tumor's side effects on the biological systems were investigated.</p> <p>Results: The results indicated that magnetic hyperthermia with microwave and linear accelerator treatment coupled with drugs was suitable for cancer treatment. A significant decrease in tumor size, tumor necrosis, and fibrosis was observed.</p> <p>Conclusion: It was found that Fe_3O_4 and Fe_2O_3-NPs coupled with MTX and exposure to photon and electron beam therapy and microwave radiation are the best methods for cancer treatment.</p>
<p>Article history: Received: Mar 12, 2020 Accepted: May 14, 2020</p>	
<p>Keywords: SEM Microwave Hyperthermia Biological Systems Linear Accelerator Histopathology</p>	

► Please cite this article as:

Abo-Neima S, Ismail A, Motaweh H. Treatment of Cancer by Radiotherapy and Nanoparticles Coupled With Methotrexate. Iran J Med Phys 2021; 18: 232-246. 10.22038/ijmp.2020.47108.1747.

Introduction

Cancer is a class of diseases resulting from unregulated cell growth; these abnormal cells can spread or invade other parts of the body [1]. Cancer remains one of the leading causes of mortality worldwide. New methods for the treatment of cancer have been successful, but the results are still limited. Hyperthermia along with conventional cancer treatments such as chemotherapy and radiation has yielded promising results [2]. Institutes aim to find innovative approaches in the world of medical sciences to solve pressing problems. For biomedical systems, those with magnetic properties are the most investigated products with promising prospects. In the last decade, the properties they have displayed on a nanometric scale have been the basis for important possible applications, such as the provision of medicines, magnetic isolation from cells or tumors, and cell labelling. Magnetic materials, especially iron oxides, have various remarkable properties, and because of their remarkable nanometric characteristics, the more common types of iron oxides,

namely hematite and magnetite (Fe_3O_4 & Fe_2O_3), are widely studied [3, 4]. Iron oxide nanoparticles are considered the best biodegradable nanomaterials that can be eliminated in the organism via normal iron metabolism pathways [5, 6]. Surface design and functional applications can be perfectly measured by nanometric materials.

In biomedical applications, nanomaterials are improved and functionalized to be used on the surface as contrast agents for magnetic resonance imaging [7, 8], tissue-specific release of therapeutic chemicals, targeted delivery of medicines for tumor therapy [9], hyperthermia, cell labelling [10], magnetic cell sortation [11], and magnetic field-assisted radionuclide therapy [12]. Over the past few years, superparamagnetic iron oxide nanoparticles have been used as contrast substances for in-vivo magnetic resonance imaging with regulated and improved surface chemical properties [13, 14]. Moreover, apart from the usage of traditional chemotherapeutic agents, various approaches to cancer inhibition have

*Corresponding Author: Tel: +98 01229631153; Email: Sahar_amr2002@yahoo.com

been investigated [1]. Photodynamic therapy using conjugated NPs in cancer treatment has been recently introduced by Jin et al. [15]. The ability of NPs as drug delivery systems in carrying drugs is 10 to 100 times higher than the molecular administration of drugs to the vicinity of tumors to improve diagnostic and therapeutic applications [16, 17].

Previous studies have focused on the development of a new drug delivery system focused on iron oxide nanoparticles to prevent damage to healthy tumor mass cells in the cancer cell death cycle. Such forms of nano systems focused on iron oxide nanoparticles can be used for heating up and providing harmful levels of thermal energy to tumors or as chemotherapy and radiotherapy-enhancing agents, where a regulated degree of tissue warmth results in active cell destruction [18, 19]. In this approach, cancerous tumors are heated to a temperature between 40°C and 45°C for a specific period, which renders tumor cells more sensitive to radiation and chemotherapy. The increase in temperature stimulates blood flow in the tumor, increases oxygenation, hence making the treatment more effective. High temperatures can kill cancer cells, but they can also injure or kill normal cells and tissues. Temperatures above 42°C can cause burns and blisters in healthy tissues. Consequently, during hyperthermia treatment, the temperature in the tumor and healthy tissue must be closely monitored [20].

Microwaves are electromagnetic radiations in the range of 300 MHz to 300 GHz [21]. Microwave hyperthermia (MH) is an electromagnetic radiation procedure raising the human body tissue temperature between 41.5°C and 45°C and preserving it within this range for a required time. Microwave hyperthermia is used for the management of superficial tumors in stand-alone or with conventional radiation and chemotherapy. In physical and sports trauma, microwave diathermy (MD) can heat tissues of the body up to 41°C. In hyperthermia, suitable applicators (antennas) are used to provide energy to penetrate the body tissues. Most of the applicators provide good energy deposition in superficial tumors [22].

In hyperthermia treatment, high-frequency electromagnetic energy is applied to the tissue using either external or internal applicators depending on the tumor location. Internal applicators use a needle or probe to release the energy directly into the tumor, and external applicators radiate the tissue from outside. Healthy tissues can also absorb the electromagnetic energy and get heated, leading to burns, blisters, and discomfort. Thus, it is critical to monitor healthy tissues' temperatures during hyperthermia treatment. Microwave hyperthermia is a non-ionizing form of radiation therapy that can greatly enhance cancer treatment effects. Because of their higher metabolism, tumor cells are considered more susceptible to the effects of hyperthermia than healthy cells [23].

One of the main approaches to the treatment of cancer is radiation treatment (RT). It is estimated that 50-60% of all cancer patients are treated with RT as either monotherapy alone or as part of a combination therapy [24, 25]. Radiation treatment uses high-energy radiation like X-rays, gamma rays, photons, protons, strong ions, and neutrons to destroy cancer cells' DNA. As both normal and cancer cells are affected by radiation therapy, care needs to be taken to mitigate the side effects. External beam radiation treatment is most often administered as light beams, including X-rays or gamma rays, from a source outside the body in contrast to internal RT or brachytherapy, which uses radioactive materials inserted into the skin next to cancer cells. The main goal of radiation therapy is to kill cancer cells while reducing damage to healthy tissues. Photons in the energy spectrum of mega-voltage and electrons up to 25 MeV are widely used for external beam therapy. This research aims to examine the effect of high-energy electrons and photons and photodynamic targeted and molecular therapies on cancer treatment.

The use of nanoparticles for cancer therapy is due to different parameters, such as their relatively small size, which contributes to longer circulation times and their ability to take advantage of tumor characteristics. For example, nanoparticles of less than 20 nm can move through the walls of blood vessels, and such a small particle size allows for intravenous, subcutaneous, and intramuscular applications. Compared to the conventional cancer treatments, the small size of nanoparticles minimizes irritant reactions at the injection site. However, the size of nanoparticles enables interactions on cell surfaces and within cells with biomolecules without altering their behaviors and biochemical properties [26].

Methotrexate (MTX) is an antimetabolite and antifolate medication used in the treatment of cancer. Methotrexate blocks DNA, RNA, and protein synthesis. This drug is cytotoxic in cell cycle's S phase. Therefore, MTX has a stronger toxic effect on the accelerated differentiation of cells (e.g., malignant and myeloid cells and gastrointestinal and oral mucosa) and more often replicates their DNA, and thus, prevents the development and proliferation of these cells and induces other side effects [27].

Complete blood count (CBC) is a standard examination used for the clinical diagnosis of several diseases, such as anemia, acute inflammation, hemorrhagic complications, allergic disorders, cancers, and immune disorders; for instance, low hematocrits is known as a marker of anemia, leucopenia, and thrombocytopenia in breast cancer patients [28], which has been supported in a study by Ufelle et al., where they reported significantly reduced levels of hematocrits, total white blood cells, and platelets in pre- and post-operative breast cancer patients [29]. Complete blood count is considered another way to limit the toxic effects of NP-based

drugs and radiotherapy by studying hematological parameters such as red blood cells (RBCs), white blood cells (WBCs), hemoglobin (Hb), packed cell volume% (PCV), mean corpuscular volume (MCV), and mean corpuscular hemoglobin concentration (MCHC) [30, 31].

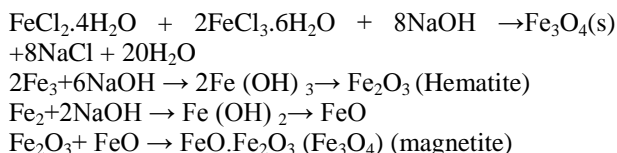
This work was conducted to evaluate the effect of high-energy photons and electrons and magnetite and hematite nanoparticles (MNP&HNPs) coupled with MTX and microwave irradiation on tumor treatment. Nanoparticles generate heat when exposed to high-energy photons and electrons. Consequently, NPs are used for magnetic fluid hyperthermia for cancer treatment and have been shown to increase the efficacy of RT coupled with MTX to overcome various practical difficulties encountered in cancer treatment and to study the effects of tumors on hematological parameters, liver and kidney functions, total antioxidant capacity, and calcium content.

Materials and Methods

Preparation of iron oxide nanoparticles (Fe_3O_4 & Fe_2O_3 -NPs)

Magnetic nanoparticles were synthesized using the wet chemical method based on the co-precipitation method. This method is based on alkaline co-precipitation of ferric and ferrous salts in an aqueous solution [32, 33]. Briefly, a solution containing Fe III at a pre-determined concentration was prepared followed by the addition of a base such as NaOH under vigorous stirring at a temperature within the range of 60–80°C. Subsequently, the solution's pH was carefully adjusted, and a dispersing element was used to stabilize the particles. All the used chemicals were procured from Sigma-Aldrich.

The chemical reaction of Fe_3O_4 and Fe_2O_3 precipitation is expected to be as follows.



Characterization of hematite and magnetite nanoparticles

As explained in the experimental part, the prepared hematite and magnetite NPs were characterized by transmission electron microscopy (TEM), scanning electron microscopy (SEM), and X-ray diffraction (XRD).

Transmission electron microscopy (TEM)

The physical size and shape of the prepared iron oxide particles was calculated by an electron microscope (JOEL JEM-2100) working at 200 kV fitted with the Erlangshen ES500 Gatan digital camera, which was carried out in Nanotech Company for photo-electronic, Dreamland, 6-October, Egypt. A drop of this MNPs solution was loaded onto a 400-mesh carbon-coated

copper grid for this purpose, allowing the solvent to evaporate in the air. Then, the solution was screened under TEM [34].

Scanning Electron Microscopy (SEM)

Scanning electron microscopes were employed to examine the morphology and appearance of dried iron oxide nanoparticles (SEM) (Jeol, JSM-6360LA, Japan). Samples were placed on a metal plate and were adhered to using silver; the samples were coated with a thin gold layer using a coater (SPI-Module TM sputter coater, Japan) [34].

X-ray Diffraction

The dried magnetic nanometers for the crystalline nature of MNPs (Shimaduz, XRD-7000, Maxima, and Japan) were analyzed using an X-ray diffractometer. With the Scherrer Equation, the size of the crystallite domain was calculated.

$$D = 0.94 \lambda / \beta \cos \theta$$

where D is perpendicular to the mirror planes to the average crystallite domain size, μ is the X-ray wavelength, β is the full width of half the maximum (FWHM), and θ is the diffraction angle. Only when the crystallite size is less than 100 nm [35] will this modified formula be applicable.

Tumor growth size measurements

The high growth rate in the Ehrlich tumor model led to a 14-day monitoring of tumor volume (V_{cm^3}) and weight (gm) in the treatment and control groups. Volume and weight of the ellipsoidal tumors were evaluated each three days, and volume (V) of the tumor was calculated using the formula below.

$$V = (\pi/6) * (L * W * H)$$

where length, width, and height are L , W , and H . Vernier caliper was used to measure tumor diameter. When the tumor reached the desired volume ($0.7 - 1 \text{ cm}^3$), the mouse was selected for treatment. The effects of time (from day 0 up to day 14) and the kind of treatment on tumor growth were examined using multivariate variance analysis (ANOVA). Multiple comparison tests were performed to determine the any significant differences between the group pairs (least significant difference). The following formula was used to estimate the tumor weight [35].

$$\text{Tumor weight (mg)} = \text{Length (cm)} \times (\text{width (cm)}^2) / 2$$

Body weight

The baseline weights of all the animals in the experiment were recorded at day Null, and the tumor mass was measured for 14 days at three-day intervals five days after injection of the tumors and then a total of 14 days each three days. The solid tumor volume was measured by a Vernier scale and determined using formula $A * B$, where A and B are the longest and shortest tumor diameters, respectively [36].

Drug used

Methotrexate provided from Borkim Chemicals and Pharmaceuticals in Alexandria (each vial contained methotrexate 50 mg, Sanofi Aventis) was administered intraperitoneally at a dosage of 2.5 mg/kg body weight [37].

Cell line

The cell line for Ehrlich ascites (EAC) was obtained from the Cairo National Cancer Institute, Egypt. Fresh Ehrlich ascites cells were cultivated in the mice with intraperitoneal (ip) sequential transfer. The 15-day EAC cells were used for testing. The screened cells were washed and suspended in phosphate-buffered saline (PBS) [37].

Hyperthermia treatment methods

Microwave treatment

The microwave unit consists of a microwave generator; this system basically includes a vacuum tube in a magnetic field to directly produce microwave energy. The cathode and anode of the magnetron had a high voltage potential difference. The output power of the magnetron was connected to the direct current of the high tensile power (Figure 1) and horn antenna (Figure 2). The microwave generator used in the present work in biophysics laboratory, Physics Department, Faculty of Science, Damanshour University, was previously described by Mohamed et al. [38]. This microwave generator produces microwave energy of the maximum continuous power of 100 W at a frequency of 2450 MHz. The applicator was placed nearly on the tumors, which was irradiated with microwave as mentioned before.

Linear accelerator treatment

Radiotherapy is the clinical process by which cancerous cells are killed using ionizing radiation. It is one of the most important medical methods used for cancer treatment. Surgery and chemotherapy are also widely used for the treatment of cancer. More than half of all cancer patients receive radiotherapy alone or in combination with surgery or chemotherapy [24, 39, 40]. The benefit of RT is that it has a potential in the nuclei of the organic tissue cells in which radiation is applied to ionize atoms and molecules, thus destroying the cancer cells with DNA damage. A linear accelerator (LINAC), as shown in Figure 3., is used for the RT system to produce ionizing radiation, which can be beams or radiographic rays (photon beams). Most treatments use X-rays or electron beam or a combination of both in RT.

For superficial tumors (less than 5 cm deep), electron beams are especially utilized; this allows for the possibility of using photon beams as well as electron beams for treating cancer in many LINAC-based RT machines. Photon beams can be generated in the range of 4-25 MV in X-ray therapy, and electron beams can be used within the range of 6-25 MeV in electron therapy. LINACs' length can range from ~30 cm for 4 to 6 MeV

LINACs to about 150 cm for 25 MeV LINACs depending on the final electron kinetic energy [41, 42].



Figure 1. A microwave generator



Figure 2. A microwave antenna



Figure 3. The linear accelerator (LINAC)

Classification of animals

Fifty-six male mice weighing approximately 20-25 g and aged 4-6 weeks were obtained from the animal house of Pharos University, Alexandria, Egypt, and were used in all the studied experiments. All the mice were housed in an environment controlled for temperature ($22 \pm 2^\circ\text{C}$) and light (12 h light/dark cycle). A suspension of 10^6 cells/ mL was prepared from Ehrlich ascites carcinoma in mice. All the experimental animals were injected into the right flank with 0.25 mL of this suspension. When tumor volume reached between 0.7 and 1 cm^3 , the mice were randomly divided

into the following groups, each group consisting of seven mice: 1st group: used as the control group injected with 25 μ L of phosphate buffer saline without treatment, 2nd group: injected with Fe₃O₄-NPs, 3rd group: injected with Fe₂O₃-NPs, 4th group: injected with methotrexate (MTX), 5th group: injected with MTX, Fe₃O₄, and Fe₂O₃-NPs, 6th group: as the 5th group with microwave hyperthermia, 7th group: as the 5th group also treated with high-energy photon radiation therapy from linear accelerator, and 8th group: as the 5th group and exposed to electron beam.

Biochemical parameter

At the end of the experiment, animals were subjected to diethyl ether anesthesia. About 2-3 mL of blood sample depending on the mice's weight was collected by heart puncture in heparinized and EDTA tubes and divided into two parts; the first part for CBC, and the other part was left for 1 hr at room temperature and then centrifuged at 3000 rpm for 15 min to separate the serum, which was kept at -20°C till used for biochemical determination like AST, ALT, urea, creatinine, calcium content, total protein, and MDA.

Hematological parameter

The following hematological parameters were tested: hemoglobin (hb) concentration, hematocrit level, erythrocyte, mean cardiac volume (MCV), mean cardiac hemoglobin (HCH), mean body concentration, and mean cardiac hemoglobin (HB). All groups of mice were anesthetized and their blood was collected into EDTA tubes for hemoglobin, red blood cell count, and white blood cell count [43]. Using heparin blood specimens, hematologic parameters were evaluated manually. Blood samples were transferred to 50- μ L hematocrit tubes and cooled at 4°C in an upright position until centrifuged (5 min at 12,000 g). Then, they were directly measured from the tubes at HCT level [44, 45]. To estimate the Hb percentage, Sahil's hemometer was used. In accordance with the formulas, RBC, HCT, and Hb erythrocyte indices, including MCV, MCH, and MCHC, were calculated [44, 45].

$$\text{MCV (fL)} = \text{HCT/RBC} (10^6/\mu\text{L})$$

$$\text{MCH (pg)} = (\text{Hb [g/L]}) / \text{RBC} (10^6/\mu\text{L})$$

$$\text{MCHC (g/dL)} = (\text{Hb [g/L]}) / \text{HCT}$$

The RBC and WBC values were calculated using the Neubauer hemocytometer (Cany Precision Instruments, Shanghai, China) in the 1:200 dilution of blood samples in Hayem solution and the 1:20 dilution of blood samples in Turk's solution, respectively [46].

Liver enzymes and kidney function

Aspartate amino transaminase (AST), alanine amino transaminase (ALT), and total protein (TP) activities were assayed using the Reitman and Frankel method [47].

Estimation of Malondialdehyde (MDA)

Malondialdehyde was measured using the Ohkawa et al. (1979) method [48]. In detail, 1 g of tissue was homogenized by 1.15% KCl in nine volumes; then, the solution was centrifuged and the supernatant was discarded. Afterwards, 1.5 mL of 20% acetic acid (pH: 3.5) and 1.5 mL of the aqueous solution of thiobarbituric acid were added to 0.2 mL of tissue homogenate/serum. The solution was rendered with distilled water up to 4 mL and then warmed for 60 min in a water bath with a glass ball as a condenser at 95°C. Subsequently, 1 mL of distilled water and 5 mL of n-butanol-pyridine mixture were added and vigorously shaken after cooling under tap water. The organic layer was taken after centrifugation at 4000 rpm for 10 min, and its absorbance was measured against a blank butanol at 532 nm. As an internal standard, TMP was used. The levels of lipid peroxide were expressed as the production of MDA in mM.

Estimation of Calcium

Serum calcium levels were estimated by the Zettner and Seligson (1964) method using an atomic absorption spectrophotometer (AAS) [49]. Serum (50 μ L) dilution with LaCl₃ was 0.01% for 40 plugs, which was mixed correctly and centrifuged at 3500 rpm for 10 min. The amount of calcium found in the supernatant was evaluated by atomic absorption spectroscopy. The stock standard was used to develop standards for different levels of calcium (0.625, 1.25, 2.5, 3.75, and 5 μ g/ml). The standards and samples against the blank solution were read. Samples, standards, and blanks were reported for their optical density. A standard curve determined the calcium content of the sera.

Histological Examination

Tumors from various groups were removed and fixed in 10% formalin for histopathological examinations. The tissue was prepared with hematoxylin and eosin as paraffin-embedded glass slides. Microscopic examination exhibited morphological changes [50].

Statistical Analysis

Analysis of variance (ANOVA) was used to analyze the data. Results are reported as mean \pm standard error (SE) and standard deviation (SD). *P*-values greater than 0.05 are considered not to be significantly different, while *P*-values less than 0.05 and 0.01 indicate significant and highly significant changes and differences, respectively.

Results

Different nanoparticle characteristics such as radius, magnetic sensitivity, and concentration were considered. The physical size and shape of the prepared iron oxide nanoparticles were determined by transmission electron microscopy (TEM).

Figures 4 and 5 show that the prepared magnetite nanoparticles were made up of crystals with a relatively

homogenous, near-spherical form. Due to their magnetic properties, particles tend to aggregate.

Iron oxide nanoparticles are evenly distributed in bright-field TEM images. Scanning electron microscopy was used to confirm the morphology of the synthesized iron oxide samples (Figures. 6 & 7). The results obtained from SEM clearly demonstrate the nearly spherical shape of the prepared magnetite nanoparticles. Due to their magnetic properties, the molecules tend to stack. As calculated by the histogram, the median particle length was ~10 nm. Electron differentiation indicated that the sample was completely crystalline, as confirmed by XRD, which showed the inverse cubic spinel structures of Fe₂O₃ and Fe₃O₄ (Figures. 8 & 9).

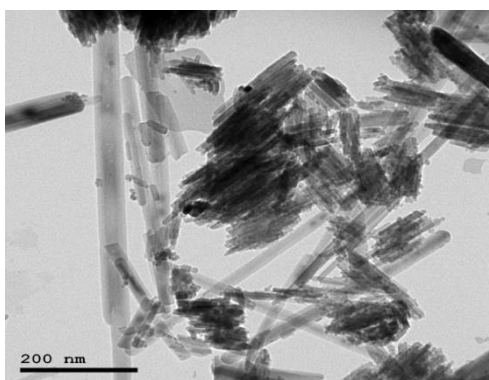


Figure 4. Transmission electron microscopy for Fe₂O₃ nanoparticles

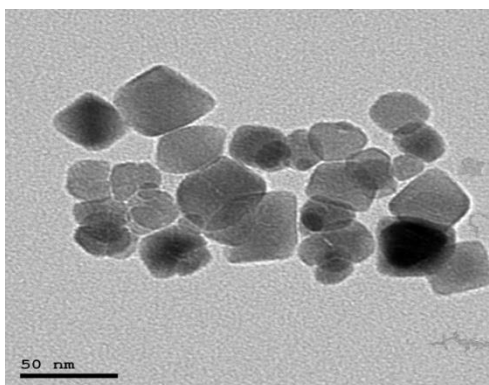


Figure 5. Transmission electron microscopy for Fe₃O₄ nanoparticles

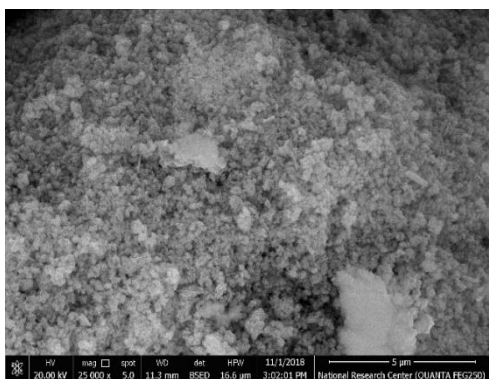


Figure 6. Scanning electron microscopy image of the synthesized iron oxide sample for Fe₂O₃ nanoparticles

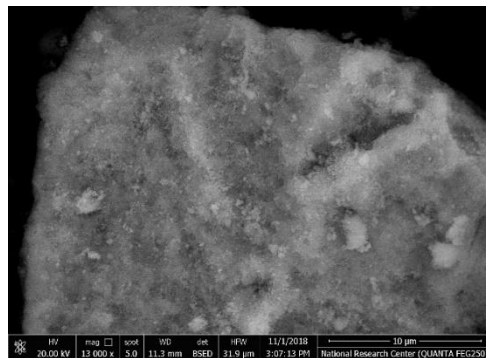


Figure 7. Scanning electron microscopy image of the synthesized iron oxide sample for Fe₃O₄ nanoparticles

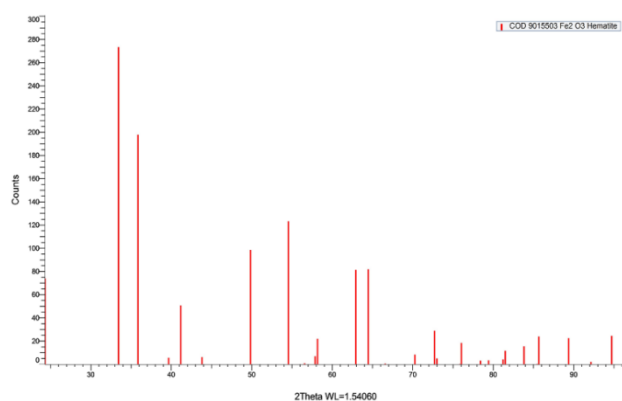


Figure 8. X-ray diffraction pattern of Fe₂O₃ nanoparticles

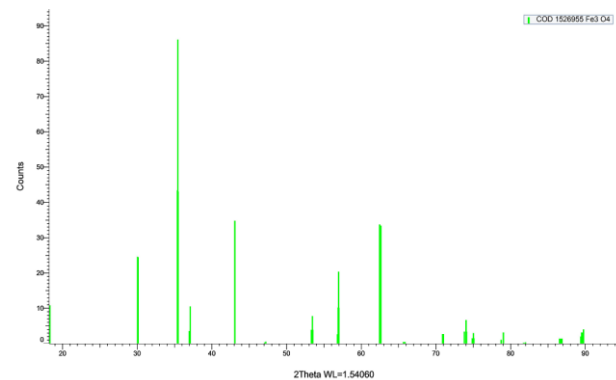


Figure 9. X-ray diffraction pattern of Fe₃O₄ nanoparticles

We studied the effect of iron oxide NPs, microwaves, photons, and electrons on liver enzymes' activity. Table 1 shows that for tumor treatment with microwave, photon, and electron, TP, AST, and ALT activity showed a highly significant reduction in liver enzymes, indicating an improvement in liver enzyme activity in these groups compared to the control group.

Table 1. Liver enzymes for all the different groups

Liver function	G ₁ (n = 7)	G ₂ (n = 7)	G ₃ (n = 7)	G ₄ (n = 7)	G ₅ (n = 7)	G ₆ (n = 7)	G ₇ (n = 7)	G ₈ (n = 7)	P
T. protein (g/ dl)	5.60–7.90	3.50–10.10	4.20–7.20	3.90–6.0	3.90–5.10	3.10–4.90	3.0–4.20	3.20–4.40	
Min – Max	6.69±0.73	6.34±2.53	5.55±1.08	4.80±0.83	4.30±0.48	3.98±0.66	3.64±0.49	3.99±0.38	
Mean ± SD	6.75	7.10	5.75	4.70	4.10	4.10	3.70	4.0	<0.001*
Median									
P _{control}		0.999	0.606	0.105	0.016*	0.004*	<0.001*	0.001*	
AST (U/ml)	98.0–185.0	161.0–195.0	151.0–205.0	88.0–118.0	53.0–87.0	47.0–62.0	36.0–52.0	42.0–54.0	
Min – Max	164.5±28.04	174.6±11.28	177.3±18.83	104.8±14.55	75.60±14.42	52.40±6.02	46.0±6.30	48.14±3.80	
Mean ± SD	174.50	171.0	180.50	113.0	81.0	51.0	49.0	48.0	<0.001*
Median									
P _{control}		0.912	0.789	<0.001*	<0.001*	<0.001*	<0.001*	<0.001*	
ALT (U/ml)	38.0–130.0	65.0–128.0	80.0–140.0	42.30–73.80	32.10–85.0	39.0–44.0	31.0–40.0	32.0–44.0	
Min – Max	87.50±27.20	103.6±19.10	108.3±25.52	51.30±12.82	54.04±19.64	41.60±1.95	35.43±3.51	39.0±4.40	
Mean ± SD	85.0	109.0	101.0	47.10	48.0	41.0	34.0	39.0	<0.001*
Median									
P _{control}		0.647	0.378	0.017*	0.035*	0.001*	<0.001*	<0.001*	

Table 2. Kidney function for all the different groups

Renal function	G ₁ (n = 7)	G ₂ (n = 7)	G ₃ (n = 7)	G ₄ (n = 7)	G ₅ (n = 7)	G ₆ (n = 7)	G ₇ (n = 7)	G ₈ (n = 7)	P
Creatinine (g/dl)									
Min – Max	0.55 – 1.40	0.65 – 1.50	0.60 – 1.10	1.50 – 1.80	1.90 – 2.50	0.33 – 0.46	0.35 – 0.60	0.24 – 0.50	
Mean ± SD	0.96 ± 0.32	1.09 ± 0.31	0.90 ± 0.19	1.62 ± 0.13	2.22 ± 0.24	0.38 ± 0.05	0.45 ± 0.09	0.40 ± 0.09	<0.001*
Median	0.90	1.20	0.90	1.60	2.20	0.36	0.42	0.41	
P _{control}		0.911	1.000	<0.001*	<0.001*	<0.001*	0.001*	<0.001*	
Urea (g/dl)									
Min – Max	44.0–58.10	43.0 – 55.0	40.0 – 69.0	66.0 – 93.0	49.0 – 87.0	35.0 – 39.0	31.0 – 44.0	30.0 – 65.0	
Mean ± SD	50.59±5.05	47.74±4.40	52.90±9.73	78.40±10.74	68.40±16.30	36.40±1.67	36.57±4.12	41.29±11.24	<0.001*
Median	50.70	47.50	52.25	80.0	70.0	36.0	37.0	39.0	
P _{control}		0.998	1.000	<0.001*	0.017*	0.106	0.059	0.449	

Table 3. Total antioxidant capacity for all the different groups

TAC	G1 (n = 7)	G2 (n = 7)	G3 (n = 7)	G4 (n = 7)	G5 (n = 7)	G6 (n = 7)	G7 (n = 7)	G8 (n = 7)	P
Min – Max	0.47 – 0.58	0.42 – 0.81	0.55 – 0.72	0.41 – 0.69	0.49 – 0.53	0.31 – 0.37	0.29 – 2.40	0.13 – 0.49	
Mean ± SD	0.52 ± 0.04	0.64 ± 0.15	0.64 ± 0.07	0.55 ± 0.13	0.51 ± 0.01	0.34 ± 0.02	0.32 ± 0.04	0.36 ± 0.11	0.476
Median	0.52	0.70	0.63	0.51	0.51	0.33	0.31	0.36	
pcontrol		0.994	0.996	1.000	1.000	0.965	0.996	0.968	

Table 4. Calcium content for all the different groups

Calcium (mmol/L)	G1 (n = 7)	G2 (n = 7)	G3 (n = 7)	G4 (n = 7)	G5 (n = 7)	G6 (n = 7)	G7 (n = 7)	G8 (n = 7)	P
Min – Max	1.80 – 3.30	2.20 – 4.70	3.90 – 6.20	4.90 – 7.30	4.10 – 7.20	8.50 – 9.10	6.90 – 8.10	6.10 – 8.80	
Mean ± SD	2.63 ± 0.52	4.03 ± 0.86	5.22 ± 0.81	5.66 ± 0.98	6.30 ± 1.28	8.86 ± 0.23	7.50 ± 0.49	7.80 ± 0.90	<0.001*
Median	2.65	4.30	5.40	5.20	6.80	8.90	7.30	7.90	
pcontrol		0.028*	<0.001*	<0.001*	<0.001*	<0.001*	<0.001*	<0.001*	

We studied the effect of iron oxide NPs, microwaves, photons, and electrons on kidney function. Data presented in Table 2 indicate that serum urea concentration showed a highly significant decrease in the group treated with magnetite, hematite, drug, and electrons (8th Group) and extremely statistically significant changes in the group treated with magnetite,

hematite, drug, and microwave (6th Group) and the group treated with magnetite, hematite, drug, and photon (7th Group). Serum creatinine concentration showed a very highly significant reduction in groups 7 and 8 and extremely statistically significant changes in Group 6 as compared to the control group. From this result we concluded that the treatment of Ehrlich tumor

with hematite and magnetite exhibits side effects on liver and kidneys functions, while for the groups treated with drug and drug with nanoparticles, side effects were solely on kidney function and not on liver function.

The results in Table 3 show a highly significant increase in TAC content for groups treated with hematite and magnetite and a very highly significant reduction in groups treated with photons, microwaves, and photons and electrons as compared to the control

group. Hematite and magnetite NPs caused TAC to increase, and magnetic NPs inhibited growth and induced apoptosis in cancer cells compared with normal cells. There were no significant changes in the groups treated with a combination of drug and nanoparticles. Table 4 displays significant adverse effects on renal function in the long-term for all the studied groups compared to the control.

Table 5. Hematological parameters in the control and experimental groups

CBC	G1 (n = 7)	G2 (n = 7)	G3 (n = 7)	G4 (n = 7)	G5 (n = 7)	G6 (n = 7)	G7 (n = 7)	G8 (n = 7)	P values
Hemoglobin concentration (g/dl)									
Min – Max	10.0–13.60	9.2–11.20	9.60–13.0	8.70–12.70	10.80–12.0	6.90–10.50	7.60–12.20	8.50–11.20	
Mean ± SD	11.70±1.22	9.87±0.66	11.30±1.34	11.14±1.59	11.46±0.98	8.26±1.40	9.70±1.40	10.20±0.98	<0.001*
Median	11.80	9.80	11.35	11.60	11.10	8.10	9.50	10.10	
pcontrol		0.094	0.999	0.991	0.698	<0.001*	0.269	0.049*	
Red Cell Count (M/ul)									
Min – Max	3.80–5.10	3.80–4.60	3.80–4.70	3.80–4.20	3.90–5.20	2.30–3.50	2.80–3.70	2.50–4.80	
Mean ± SD	4.39±0.50	4.14±0.26	4.27±0.37	3.96±0.18	4.41±0.51	2.74±0.47	3.40±0.32	3.64±0.76	<0.001*
Median	4.25	4.10	4.20	3.90	4.30	2.70	3.40	3.80	
pcontrol		0.969	1.000	0.739	1.000	<0.001*	0.004*	0.062	
Haematocrit (PCV) (%)									
Min – Max	31.0–40.0	28.60–34.60	29.80–38.50	27.10–38.80	36.40–48.40	21.70–32.50	26.50–34.60	23.80–37.60	
Mean ± SD	35.88±3.29	30.77±2.04	34.65±3.67	34.36±4.70	40.78±4.94	25.78±4.21	31.63±2.94	30.26±4.15	<0.001*
Median	36.401	30.40	35.05	35.80	38.50	25.30	31.40	29.50	
pcontrol		0.166	0.999	0.996	0.309	0.001*	0.368	0.094	
M.C.V (fL)									
Min – Max	74.30–91.60	70.20–77.50	74.50–86.60	85.50–94.20	89.50–93.50	92.80–95.40	92.20–94.60	67.70–95.20	
Mean ± SD	82.14±6.88	74.29±2.44	81.17±3.89	91.60±3.49	92.39±1.65	94.16±0.98	93.03±0.89	84.83±11.29	<0.001*
Median	81.95	75.20	81.75	92.60	93.07	94.30	92.80	92.20	
pcontrol		0.136	1.000	0.076	0.042*	0.009*	0.009*	0.980	
M.C.H (Pg)									
Min – Max	24.0–29.60	22.60–24.50	24.0–28.10	26.70–30.50	29.10–30.40	30.0–30.40	22.80–40.80	29.70–30.40	
Mean ± SD	26.55±2.23	23.81±0.70	26.28±1.32	29.45±1.55	30.01±0.52	30.16±0.22	29.71±5.85	30.01±0.32	<0.001*
Median	26.65	24.20	26.45	30.0	30.20	30.0	30.04	30.0	
pcontrol		0.425	1.000	0.475	0.258	0.212	0.252	0.160	
M.C.H.C (g/dl)									
Min – Max	32.30–34.0	31.40–32.40	32.20–33.20	32.10–32.70	32.40–32.60	31.80–32.30	32.10–32.40	31.10–32.90	
Mean ± SD	32.60±0.57	32.09±0.32	32.50±0.36	32.38±0.22	32.48±0.08	32.02±0.19	32.26±0.11	32.14±0.55	0.065
Median	32.45	32.20	32.40	32.40	32.50	32.0	32.20	32.20	
pcontrol		0.163	1.000	0.966	0.999	0.143	0.284	0.639	

p: P-value for comparing between the studied groups,
 p_{control}: P-value for comparing between the control group and the other groups
 *: Statistically significant at p≤ 0.05

The most common hematological effect of cancer is anemia (decrease in Hb value, PCV, and RBCs count). The reduced RBC, PCV, and Hb is because RBCs are derived from hemopoietic stem cells in the bone marrow. Following a series of maturation steps, directed mainly by erythropoietin, red blood cells enucleate and enter the circulatory system; therefore, the alteration in RBCs can be related to the hematopoietic system.

Table 5 shows significant changes in all the complete blood count parameters, clearly demonstrating a lack of cytotoxic effects. Hematological parameters are frequently used in routine tests for the diagnosis of many diseases, such as infections, anemia, allergy, immune disfunctions, cancer, and numerous other diseases. Hemoglobin and RBC were decreased for the

treated groups (p -value < 0.001), while PCV was lower in all the groups than the control group.

Relative volume and variation of weight of the tumors in each group at the end of the treatment period (9 days) are shown in Table 6. The figures show that the volume and weight of the tumors in comparison with the control group were very significantly reduced in different treatment groups. The results indicated that the treatment of cancer by photon combined with chemotherapy and nanoparticles induced the most tumor growth inhibition.

Table. 6. Tumor size and weight for all the groups

Groups	Tumor volume (cm ³) after 15 day	Tumor weight (gm)
G1	0.13	0.29
G2	0.11	0.32
G3	0.14	0.32
G4	0.12	0.30
G5	0.093	0.167
G6	0.05	0.15
G7	0.019	0.05
G8	0.03	0.1

Histopathological examination of the Ehrlich solid tumor (EST) under light microscope was performed for all the groups studied under the same conditions, and the

results were compared with mice bearing tumors. We found that the groups treated with magnetite, hematite, and MTX showed similar results in histopathological examination compared with the untreated tumor-bearing mice. Figure 10 shows the invasion of subcutaneous adipose tissue and skeletal muscles (*) by neoplastic cells (yellow arrows); the tumor capsule is infiltrated by inflammatory cells. Hemorrhagic regions and necrotic areas (black arrows) are also detectable. Numerous newly-formed blood capillaries (neovascularization) are seen in the surrounding tissue with mild or no inflammatory infiltration (Scale bar: 200, 400 μ m). Figure 11 exhibits mice treated with Fe₃O₄, Fe₂O₃-NPs, MTX, and photon radiation therapy, which caused minimal tumor cell infiltrations, such that the skin hair follicles with their associated sebaceous glands are observable (double black arrows). Few numbers of round cells of mostly lymphocytes and macrophages seems to be normal. Figure 12 is about mice treated with nanoparticles and drug (MTX) and shows similar degrees of infiltration compared to the untreated tumor-bearing mice (control group). Similar areas of necrosis and newly formed blood capillaries (black arrows) are also noticed. Inflammatory cell infiltration and necrosis in comparison with EST were slightly increased.

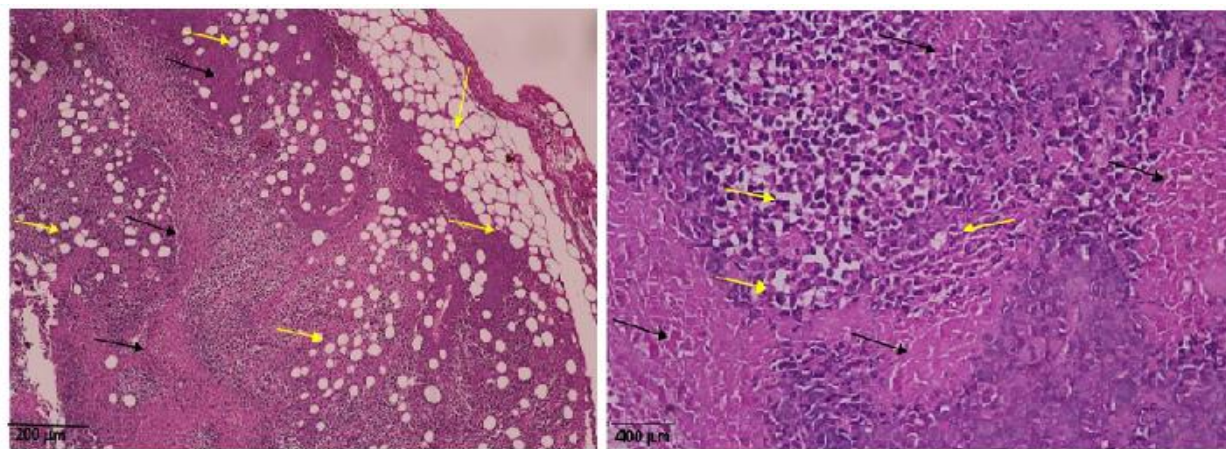


Figure10. Untreated tumor bearing-mice stained with hematoxylin and eosin (H&E), showing the invasion of subcutaneous adipose tissue and skeletal muscles (*) by the neoplastic cells (yellow arrows); the tumor capsule is infiltrated by inflammatory cells. Hemorrhagic regions and necrotic areas (black arrows) are also detectable. Numerous newly formed blood capillaries (neovascularization) are seen in the surrounding tissue with mild or no inflammatory infiltration (Scale bar: 200, 400 μ m)

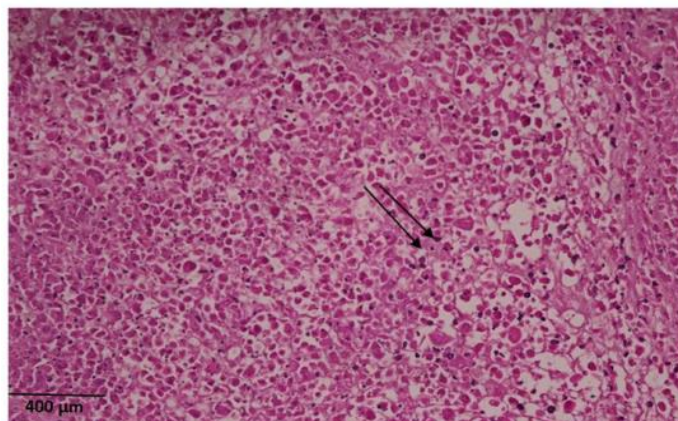


Figure 11. Mice treated with Photons + Drug + Fe_3O_4 -NPs + Fe_2O_3 -NPs stained with hematoxylin and eosin (H&E), reveals minimal tumor cell infiltrations, such that the skin hair follicles with their associated sebaceous glands are seen (double black arrows). Few numbers of round cells of mostly lymphocytes and macrophages seems to be normal. (Scale bar: 400 μm).

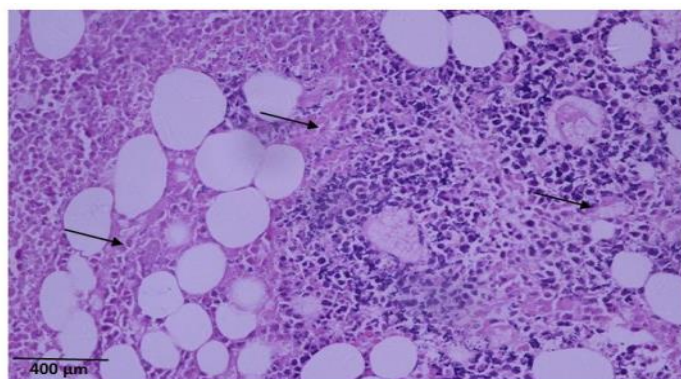


Figure 12. Mice treated with nanoparticles and methotrexate (MTX) stained with hematoxylin and eosin (H&E), shows a similar degree of infiltration compared to the untreated tumor-bearing mice (control group). Similar areas of necrosis and newly formed blood capillaries (black arrows) are also noticed. Inflammatory cells infiltration and necrosis in comparison with EST were slightly increased (Scale bar: 400 μm).

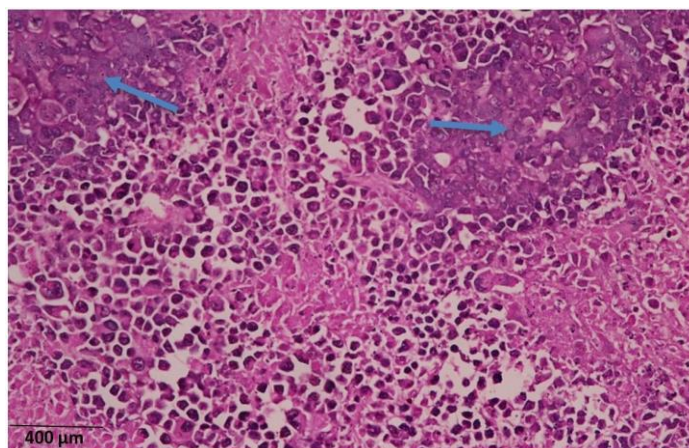


Figure 13. Mice treated with MW + Drug + Fe_3O_4 -NPs + Fe_2O_3 -NPs stained with hematoxylin and eosin (H&E), showing compact aggregation of the tumor tissue cells (blue arrows) and a similar degree of infiltration as described for untreated tumor-bearing mice (control). Inflammatory cellular infiltration and necrosis in comparison with EST are increased (Scale bar: 400 μm).

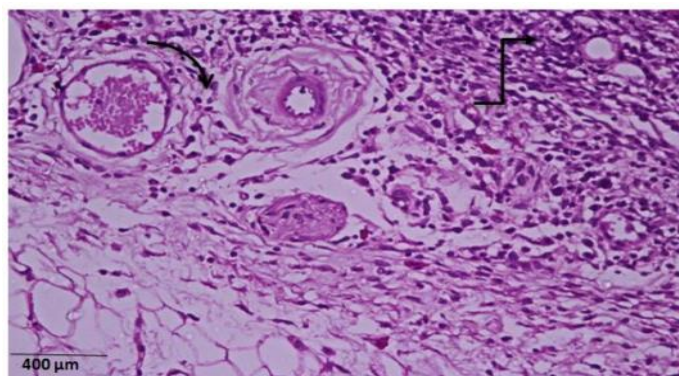


Figure 14. Mice treated with Electrons+ Drug + Fe_3O_4 -NPs + Fe_2O_3 -NPs stained with hematoxylin and eosin (H&E), revealing limited foci of tumor cells (elbow arrow) in comparison with ESTs treated with photons. Inflammatory cells and necrosis are minimal. Increased vascularity of the surrounding subcutaneous tissue (curved arrow) is evident (Scale bar: 400 μm).

Figure 13 concerns mice treated with Fe_3O_4 , Fe_2O_3 -NPs, MTX, and microwave hyperthermia and shows compact aggregation of the tumor tissue cells (blue arrows), which indicates a similar degree of infiltration as described for the untreated tumor-bearing mice (control). Inflammatory cellular infiltration and necrosis in comparison with EST were increased. Finally, Figure 14 is about mice treated with Fe_3O_4 , Fe_2O_3 -NPs, MTX, and electron beam therapy and reveals the limited foci of tumor cells (elbow arrow) in comparison with EST treated with photons. Inflammatory cells and necrosis were minimal, and increased vascularity of the surrounding subcutaneous tissue (curved arrow) is evident.

Discussion

The incidence of human cancer has increased dramatically over the last 30 years [51, 52]; however, there is a paucity of data on the clinical effects of chemotherapy and its serious side effects, therapeutic efficacy, and multidrug resistance [53, 54]. Combination therapy is one of the main methods for treating cancer in view of the above obstacles. Its significant advantage is that synergy can be achieved not only through different cell cycle stages and mechanisms but also by suppressing drug resistance to harm or kill cancer cells with multiple drugs. Methotrexate is a broad-speed, effective, chemical therapeutic drug for the treatment of a wide range of human cancers, including cervical, mammalian, lung, head, neck, and skin malignant tumors [58, 59]. The dihydrofolate reductase enzyme involved in folate metabolism can be inhibited by MTX [60]. The clinical application of MTX is, however, limited because of poor pharmacokinetics and severe systemic toxicity after systemic administration [61, 62].

In the developed countries, cancer remains one of the main causes of death. There are various disadvantages to conventional cancer therapies such as surgery, radiation, chemotherapy, and biopsy. Some of these drawbacks include tumor accessibility, operative risk for vital organs, spread of cancer cells throughout the body, and lack of selectiveness for tumor cells. In

the treatment of small tumors, immunotherapy has been applied since its effectiveness decreases during later stages of cancer. In order to provide a better chance for survival, multimodal therapy has been used [63].

Cancer is an abnormal growth of cells, which in certain cases, leads to metastases and uncontrolled growth. It can cause death immediately if left untreated. Nanotechnology may chemically, physically, and biologically enhance selective approaches to cancer cell death, while minimizing non-malignant cell toxicities [6]. Cobalt, nickel, and iron nanoparticles are magnetic elements and are used for the treatment of cancer by functionalizing therapeutic drug surfaces like MTX, drug tracing, and analyzing radionuclides, genetic materials such as SiRNA for targeted gene therapy, and tumor immunotherapy antibodies [6]. Under a theragnostic platform leading to multimodal treatment of cancer, magnetic NPs, which can be possibly used in imaging and treating hyperthermia [64], are considered. Medicines can precisely target cell tissues and types by using magnetic nanoparticles (MNPs) as a medication system.

This study describes the usual MNPs' synthetic strategies and includes payload drugs for MNPs, which have benefits like visual focusing and delivery. In addition, the application of MNPs increased the efficiency and safety of the drug delivery process.

Inorganic NPs can also be classified as metal-based NPs. Due to their therapeutic and imaging properties, the capabilities of such inorganic NPs have been thoroughly investigated in the last decade. The bulk of these NPs shares the same kind structure containing a core, which is responsible for the electronic, magnetic, and optical properties, and a shell, which is mainly an organic surface coating. Among them, the most widely used metal-based NPs for cancer treatment are Fe_3O_4 -NPs and Fe_2O_3 -NPs. The use of NPs in cancer therapy increases drug solubility, increasing the bioavailability of many chemotherapeutic medicines [65, 66]. Nanoparticles may also increase accumulation by enhanced permeability and retention of drugs in cancer tissues [67]. In the end, the combination of NPs-anti-cancer medicines can improve therapy efficiency by

reducing side-effects and using goal ligands to target specific tumor sites [68, 69].

With increased interest in magnetic nanoparticles owing to their magnetic, electronic, optic, and chemical properties due to extremely their small sizes and large specific surface areas, MNPs of various compositions, sizes, and shapes have become an active research field in the area of magnetism. They have many potential applications in electronics, opto-electronics, and data storage. Owing to their ease of preparation, strong ferromagnetic behavior, and oxidative stability (less sensitive to oxidation than magnetic transition metals such as Co, Fe and Ni), major interest has recently been devoted to the synthesis of iron oxide magnetic NPs such as magnetite and hematite, which have received the most attention for biomedical applications [70, 71].

A study on enhanced cancer hyperthermia with magnetic nanoparticles is discussed in this dissertation. Hyperthermia has been used for a long time to increase tumor temperature by about 42°C without damaging the surrounding healthy tissues as a possible alternative method in cancer treatment. In this method, high-frequency microwave and high-energy photons and electrons are used. Magnetic fluid hyperthermia involves injecting energy-rich photons and electrons of magnetic nanoparticles into the tumor before exposure to microwave irradiation. Nanoparticles transform magnetic energy into heat that enables a quicker temperature rise in the tumor to the desired level. The new multidisciplinary approach to cancer therapy is one of the most exciting. The electrical membrane potential and the electrical impedance of cancer cells are both smaller than the normal cell potential. As injured and cancerous cells do not maintain normal membrane potential, it will prevent repair of metabolic functions and their return to normal. Therefore, the restoration of healthy membrane potential within cells would be a key component of cell repair and cancer treatment [72].

The primary goal of the work was to assess the capacity of nanoparticles to transform electromagnetic energy into therapeutic heating for photons, electrons, and microwave frequencies. The temperature of the targeted zone over the peripheral region can be increased with targeted nanoparticles together with microwave irradiation. To become clinically viable, it is therefore necessary to identify a microwave that absorbs no particles and to develop a treatment monitoring system.

Nanomaterials have revolutionized the process of localized heating by means of photothermal procedures. Localized heating by non-radiative radiation may kill cancer cells more effectively; thus, nanomaterials can have a promising impact. Nanomaterials are internalized into tumor sites and are stimulated by the application of frequencies, leading to localized temperature surge. Nanomaterials are also used for reactive oxygen species generating photodynamic therapy [6] under photon-beam electron irradiation. Consequently, the functionalization of nanoparticles with cytotoxic drugs and microwave and electron beam therapy is the best

method to damage tumors. Aspartate transaminase (AST), alanine transaminase (ALT), and alkaline phosphatase are the most important parameters that can be used in determining the hepatotoxic effects of MNPs. Alanine transaminase and AST are two of the most reliable markers of hepatocellular injury or necrosis. In several hepatic disorders, their levels can be elevated. Alanine transaminase is thought to be more specific to liver injury, since it is mainly found in liver cytosol and elsewhere in low levels. Aspartate transaminase is in cytosolic and mitochondrial shapes and is present in liver tissue. Alkaline phosphatase (ALP), which is present in liver tissue, is a marker of hepatic diseases or bone disorders. According to our histopathological study, MNPs and HNPs coupled with MTX and exposed to high-energy photons and electron are the best methods for cancer treatment.

Conclusion

1. It was found that magnetic nanoparticles enter tumor tissue, spread, and remain in the tumor tissue and help to eliminate cancer cells by using various treatment methods, while they do not affect normal cells.
2. It was found that cancer increased total protein, AST, and ALT activities. It also affected the functions of the kidneys as evidenced by the increased concentrations of urea and creatinine.
3. Ehrlich's treatment with hematite, magnetite, drug, and drug + nanoparticles adversely affected liver and kidney functions, except for the photons, electrons, and microwave + nanoparticles treatment, which improved the liver and kidney functions in comparison to the untreated tumor-bearing mice (Control).
4. Hematite and magnetite magnetic nanoparticles caused TAC to increase, and they inhibited the growth and induced apoptosis in cancer cells in the long-term compared to normal cells.
5. A histopathological study of Ehrlich tumors in photons, electrons, and microwave + nanoparticles groups showed tumor necrosis and fibrosis.
6. The normalized tumor size was decreased with different treatment methods compared to the untreated tumor-bearing mice (Control), which was highly significant. The extremely dramatic decline in the growth of cancer cells as a result of photon treatment was also noted.
7. In groups where a combination of microwave + nanoparticles and electrons were used, statistically significant differences were obtained.
8. It was found that hematite and magnetite coupled with MTX and exposure to high energy photons and electrons is the best method for cancer treatment.

Acknowledgment

Many thanks are directed to Dr. Sabbah I. Hammoury, Department of Medical Physics, Alexandria Ayadi Almostakbl Oncology Center, Alexandria, Egypt, for providing us the Linear Accelerator (LINAC) radiotherapy system to produce high-energy photon and electron beams.

References

- Piumi Y, Liyanage D, Hettiarachchi Z, Allal Ouhtit, Elif S, Cagri O, et al. Nanoparticle-mediated targeted drug delivery for breast cancer treatment. *Biochim Biophys Acta Rev Cancer*. 2019 April; 1871(2): 419-33.
- Wust P, Hildebrandt B, Sreenivasa G, Rau B, Gellermann J, Riess H, et al. Hyperthermia in combined treatment of cancer. *Lancet Oncol*. 2002; 3: 487-7.
- Laurent S, Forge D, Port M. Magnetic iron oxide nanoparticles: synthesis, stabilization, vectorization, physic chemical characterizations and biological applications. *Chemical Reviews*. 2008;108(6): 2064-10.
- Laurent S, Dutz S, Hafeli UO, Mahmoudi M. Magnetic fluid hyperthermia: focus on superparamagnetic iron oxide nanoparticles. *Advances in Colloid and Interface Science*. 2011; 166(1-2): 8-23.
- Nosrati H. Anticancer activity of tamoxifen loaded tyrosine decorated biocompatible Fe₃O₄ magnetic nanoparticles against breast cancer cell lines. *J Inorg Organomet Polym Mater*. 2018;28(3):1178-86.
- Sanjay K, Pratibha K, Rajeev S Emerging. Nanomaterials for Cancer Therapy. *Nanoparticles in Medicine*. 2020: 25-54.
- Cunningham CH, Arai T, Yang PC, McConnell MV, Pauly JM, Conolly SM. Positive contrast magnetic resonance imaging of cells labeled with magnetic nanoparticles. *Magnetic Resonance in Medicine*. 2005;53(5): 999-05.
- Anderson SA, Rader R K, Westlin WF. Magnetic resonance contrast enhancement of neovasculature with alpha(v)beta(3)-targeted nanoparticles. *Magnetic Resonance in Medicine*. 2000;44 (3): 433-9.
- Polyak B, Friedman G. Magnetic targeting for site-specific drug delivery: applications and clinical potential. *Expert Opinion on Drug Delivery*. 2009 ;6(1): 53-70.
- Weissleder R, Cheng HC, Bogdanova A, Bogdanov A. Magnetically labeled cells can be detected by MR imaging. *Journal of Magnetic Resonance Imaging*. 1997;7(1):258-63.
- Schellenberger EA, Reynolds F, Weissleder R, Josephson L. Surface-functionalized nanoparticle library yields probes for apoptotic cells. *ChemBioChem*. 2004;5(3):275-79.
- Jalilian AR, Panahifar A, Mahmoudi M, Akhlaghi M, Simchi A. Preparation and biological evaluation of [67Ga]-labeled- superparamagnetic nanoparticles in normal rats. *Radiochimica Acta*. 2009 ;97(1): 51-6.
- Corot C, Robert P, Idee JM, Port M. Recent advances in iron oxide nanocrystal technology for medical imaging. *Advanced Drug Delivery Reviews*. 2006;58(14): 1471-04.
- Fan C, Gao W, Chen Z. Tumor selectivity of stealth multi-functionalized superparamagnetic iron oxide nanoparticles. *International Journal of Pharmaceutics*. 2011; 404(1-2): 180-90.
- Jin G, He R, Liu Q, Dong Y, Lin M, Li W, Xu F. Theranostics of triple-negative breast cancer based on conjugated polymer nanoparticles. *ACS Appl. Mater. Interfaces*2018;10 :10634-46.
- Park K, Lee S, Kang E, Kim K, Choi K, Kwon IC. New generation of multifunctional nanoparticles for cancer imaging and therapy. *Adv Funct Mater*. 2009;19(10):1553-66.
- Atefeh R, Ameneh S. Gold nanoparticles as cancer theranostic agents. *Nanomed J*. 2019; 6(3): 147-60.
- Pankhurst QA, Connolly J, Jones SK, Dobson J. Applications of magnetic nanoparticles in biomedicine. *Journal of Physics D*.2003;36(13):167-81.
- Gilchrist R K, Shorey WD, Hanselman RC, Parrott JC, Taylor CB. Selective inductive heating of lymph. *Annals of Surgery*.1957; 146: 596-06.
- Lee ER. Electromagnetic superficial heating technology. *Thermo radiotherapy and thermo chemotherapy*, Springer-Verlag. 1995:193-17.
- James C L. *Advances in Electromagnetic Fields in Living Systems*. Springer Science Business Media.2005; 14: 59.
- Wust S. *Electromagnetic deep heating technology, Thermo radiotherapy and thermo chemotherapy*. Springer-Verlag.1995:219-51.
- Linh PH, Thach PV, Tuan NA, Thuan NC Manh DH, Phuc NX. Magnetic fluid based on Fe₃O₄ nanoparticles: Preparation and hyperthermia application. *Journal of Physics*. 2009; 187: 1-5.
- Delaney G, Jacob S, Featherstone C, Barton M. The role of radiotherapy in cancer treatment: estimating optimal utilization from a review of evidence-based clinical guidelines. *Cancer*.2005; 104: 1129-37.
- Schaefer D, Bridge WH. Opportunities and challenges of radiotherapy for treating cancer. *Nat. Rev.Clin. Oncol*. 2015;12:527-40.
- Vaishnava PP. Magnetic relaxation and dissipative heating in ferrofluids. *Journal of Applied Physics*. 2007; 102.
- Katz E, Willner I. Integrated nanoparticle-biomolecule hybrid systems: synthesis, properties, and applications. *Angewandte Chemie*.2004;43(45): 6042-08.
- Ali LO. Study effect of breast cancer on some hematological and biological parameters in Babylon province. *Iraq Journal Pharmacy and Biological Sciences*. 2014; 9: 20-24.
- Ufelle SA, Ukaejiofo EO, Neboh EE, Achukwu P U, Ikekpeazu E J, Maduka I C, et al. Some haematological parameters in pre-and post- surgery breast cancer patients in Emugu, Nigeria. *Int J Cur Bio Med Sci*. 2012; 2: 188-90.
- Abdelhalim MA, Moussa SA. The dimensional hematological alteration induced in blood of rats in vivo by intraperitoneal administration of gold nanoparticles. *Nanomed and Nanotechnol*.2012; 3:138.

31. JoMR, BaeSH, GoMR, KimHJ, HwangYG, hoiSJ. Toxicity and biokinetics of colloidal gold nanoparticles. *Nanomaterials*.2015; 5:835-50.
32. Palacin PC, Hidber J, Bourgoin C, Miramond C, Fermon and G. Whitesides. Patterning with magnetic materials at the micron scale. *Chem.Mater*.1996; 8:1316-25.
33. Enzel p, Adelman NB, Beckman KJ, Campbell DJ, Ellis AB, Lisensky GC. Preparation and Properties of an Aqueous Ferrofluid. *J. Chem. Educ.* 1999;76: 943.
34. Linh PH, Van Thach P, Tuan NA, Thuan NC, Phuc NX. Magnetic fluid based on Fe₃O₄ nanoparticles: Preparation and hyperthermia application. In *Journal of Physics: Conference Series* 2009 Sep 1; 187(1): 012069.
35. Jaganathan SK, Mondhe D, Wani ZA, Pal HC, Mandal M. Effect of honey and eugenol on Ehrlich ascites and solid carcinoma. *Journal of Biomedicine and Biotechnology*. 2010 Oct;2010.
36. Reilly MS, Boehm T, Shing Y. Endostatin: an endogenous inhibitor of angiogenesis and tumor growth. *Cell*.1997;88(2):277-85.
37. Mohamed NA, Ahmed MK. Comparative study between the effect of methotrexate and valproic acid on solid Ehrlich tumour. *Journal of the Egyptian National Cancer Institute*.2012; 24(4):161-7.
38. Mohamed MM, UchidaT, Minami S. A pulse operated microwave induced plasma source. *Spectrosc*. 1989;43: 129 37.
39. Begg C, Stewart A, Vens C. Strategies to improve radiotherapy with targeted drugs. *Nat Rev Cancer*. 2011; 11:239-53.
40. Rajamanickam B, Kuo L, Richard Y and KhengW. Cancer and Radiation Therapy: Current Advances and Future Directions. *Int. J. Med. Sci.* 2012; 9(3):193-9.
41. Hanna S. RF Linear Accelerators for Medical and Industrial Applications. Artech House Publishing. 2012.
42. Podgorsak EB. Radiation Oncology Physics: A Handbook for Teachers and Students. Vienna: International Atomic Energy Agency (IAEA);2005.
43. Ramnik S. Medical Laboratory Technology: methods and Interpretations. 5th ed. Jayee Brothers. New Delhi. 1999.
44. Gao ZX, Wang WM, Abbas K, Zhou XY, Yang Y, Diana JS, Wang H P, Wang HL, Li Y, Sun YH. Haematological characterization of loach *Misgurnus anguillicaudatus*: comparison among diploid, triploid and tetraploid specimens. *Comparative Biochemistry and Physiology, Part A: Molecular & Integrative Physiology*. 2007a;147(4):1001-08.
45. Gao ZX, Wang WM, Yang Y, Abbas K, Li DP, Zuo GW, Diana JS. Morphological studies of peripheral blood cells of the Chinese sturgeon, *Acipenser sinensis*. *Fish Physiology and Biochemistry*.2007b; 33:213-22.
46. Cao XY, Wang WM. Haematological and biochemical characteristics of two aquacultured carnivorous cyprinids, topmouth culter *Culter alburnus* (Basilewsky) and yellowcheek carp *Elopichthys bambusa* (Richardson). *Aquaculture Research*. 2010; 41: 1331-38.
47. Reitman S, Frankel S. Glutamic - Pyruvate Transaminase Assay by Colorimetric Method. *Am. J. Clin.* 1957; Path 28: 56.
48. Ohkawa H, Ohishi N, Yagi K. Assay of lipid peroxides in animal tissues by thiobarbituric acid reaction. *Annals of Biochemistry*. 1979; (95):351-58.
49. Zettner A. Seligson. Application of atomic absorption spectrophotometry in the determination of calcium in serum. *Clin. Chem.* 1964;10: 869-89.
50. Su B, Xiang SL, Su J. Diallyl disulfide increases histone acetylation and P21WAF1 expression in human gastric cancer cells in vivo and in vitro. *Biochemical Pharmacology*. 2012; 1(7):1-10.
51. Siegel L, Miller D, Jemal A. Cancer statistics. *CA Cancer J Clin.* 2016; 66:7-30.
52. Jiajiang X, Zhongxiong F, Yang l, Yinying Z, Fei Y, guanghao S, et al. Design of pH-sensitive methotrexate prodrug-targeted curcumin nanoparticles for efficient dual-drug delivery and combination cancer therapy. *International Journal of Nanomedicine*. 2018; 13:1381-98.
53. Brigger I, Dubernet C, Couvreur P. Nanoparticles in cancer therapy and diagnosis. *Adv Drug Deliv Rev.* 2002; 54:631-51.
54. Wu Q, Yang Z, Nie Y, Shi Y, Fan D. Multi-drug resistance in cancer chemotherapeutics: mechanisms and lab approaches. *Cancer Lett.* 2014; 347:159-66.
55. Lehár J, Krueger AS, Avery W, Heilbut AM, Johansen LM, Price ER, et al. Synergistic drug combinations tend to improve therapeutically relevant selectivity. *Nature biotechnology*. 2009 Jul;27(7):659-66.
56. Liu Z, Jiao Y, Wang Y, Zhou C, Zhang Z. Polysaccharides-based nanoparticles as drug delivery systems. *Adv Drug Deliv Rev.* 2008; 60:1650-62.
57. Song L, Pan Z, Zhang H, et al. Dually folate/Cd44 receptor-targeted self-assembled hyaluronic acid nanoparticles for dual-drug delivery and combination cancer therapy. *J Mater Chem B.* 2017; 5:6835-46.
58. Thomas TP, Huang B, Choi SK, Silpe JE, Kotlyar A, Desai AM, et al. Polyvalent dendrimer-methotrexate as a folate receptor-targeted cancer therapeutic. *Molecular pharmaceutics*. 2012 Sep 4;9(9):2669-76.
59. Zeb A, Qureshi OS, Kim HS, Cha JH, Kim HS, Kim JK. Improved skin permeation of methotrexate via nanosized ultradeformable liposomes. *Int J Nanomedicine*. 2016;11:3813-24.
60. Boechat AL, de Oliveira CP, Tarragô AM, da Costa AG, Malheiro A, Guterres SS, et al. Methotrexate-loaded lipid-core nanocapsules are highly effective in the control of inflammation in synovial cells and a chronic arthritis model. *International journal of nanomedicine*. 2015;10:6603.
61. Mount C, Featherstone J. Rheumatoid arthritis market. *Nat Rev Drug Discov.* 2005;4:11-12.
62. Shao Z, Shao J, Tan B, Guan S, Liu Z, Zhao Z, et al. Targeted lung cancer therapy: preparation and optimization of transferrin-decorated nanostructured lipid carriers as novel nanomedicine for co-delivery of anticancer drugs and DNA. *International journal of nanomedicine*. 2015; 10:1223.

63. Rex DK, Kahi CJ, Levin B, Smith RA, Bond JH, Brooks D. Guidelines for colonoscopy surveillance after cancer resection: a consensus update by the American Cancer Society and the US Multi-Society Task Force on Colorectal Cancer. *Gastroenterology*. 2006; 130(6):1865-71. DOI: 10.1053/j.gastro.2006.03.013
64. Bonvin D, et al. Folic acid on iron oxide nanoparticles: platform with high potential for simultaneous targeting, MRI detection and hyperthermia treatment of lymph node metastases of prostate cancer. *Dalton Trans*. 2017;46(37):12692-704.
65. Peer D, Karp JM, Hong S, Farokhzad OC, Margalit R, Langer R. Nanocarriers as an emerging platform for cancer therapy. *Nature nanotechnology*. 2007 Dec;2(12):751-60.
66. Wang X, Yang L, Chen Z, Shin DM. Application of nanotechnology in cancer therapy and imaging, CA: *Cancer J. Clin*. 2008; 58: 97-110.
67. Fang J, Nakamura H, Maeda H, The EPR effect: Unique features of tumor blood vessels for drug delivery, factors involved, and limitations and augmentation of the effect. *Adv. Drug Deliv*. 2011; 63:136-51.
68. Gong J, Chen M, Zheng Y, Wang S, Wang Y. Polymeric micelles drug delivery system in oncology. *J. Control. Release*. 2012; 159 :312-23.
69. Cheng R, Meng F, Deng C, Klok H-A, Zhong Z. Dual and multi-stimuli responsive polymeric nanoparticles for programmed site-specific drug delivery. *Biomaterials*. 2013; 34: 3647-57.
70. Nedkov T, Merodiiska L, Slavov RE, Vandenberghe Y, Kusano J, Takada J. Surface oxidation, size and shape of nano-sized magnetite obtained by co-precipitation. *Magn. And Magn. Mater*. 2006 ;300(2): 358-67.
71. Cengelli F. Interaction of functionalization superparamagnetic iron oxide nanoparticles with brain structures. *Journal Of Pharmacology And Experimental Therapeutics*. 2006; 318: 108-16. DOI:10.1124/ipet.106.101915.
72. Rasha SS, Mohamed MM, Tayel MB, Ali NH. Effect of microwave hyperthermia on tumor treatment. *Romanian J. Biophys*. 2013; 23(4): 249-59.